Hindawi
International Journal of Mathematics and Mathematical Sciences
Volume 2022, Article ID 7987315, 16 pages
https://doi.org/10.1155/2022/7987315

Research Article

A Numerical Study on Newtonian Heating Effect on Heat Absorbing MHD Casson Flow of Dissipative Fluid past an Oscillating Vertical Porous Plate

B. Prabhakar Reddy and L. Joseph Sademaki

Department of Mathematics and Statistics, CNMS, the University of Dodoma, P. O. Box 338, Dodoma, Tanzania

Correspondence should be addressed to B. Prabhakar Reddy; prabhakar.bijjula@gmail.com

Received 18 August 2021; Revised 20 January 2022; Accepted 17 February 2022; Published 29 March 2022

Academic Editor: Hans Engler

The numerical study of Newtonian heating effect on unsteady free convection MHD Casson flow of radiating and chemically reacting fluid past an oscillating vertical porous plate embedded in a porous medium was conducted by considering the effects of heat sink and viscous dissipation. The fluid motion is persuaded due to the periodic oscillations of the plate along its length. This phenomenon is represented as nonlinear PDEs with initial and boundary conditions. By introducing suitable nondimensional variable and parameters, the leading equation with initial and boundary conditions is converted into dimensionless form, which are then solved numerically using a finite difference method. The effects of several relevant parameters on the velocity, temperature, and concentration are displayed graphically, whilst the effects of these parameters on the skin friction and Nusselt and Sherwood numbers are exhibited in tabular format and then discussed in detail. The final outcomes divulge that the radiation parameter and Eckert number have an increasing effect on the velocity and temperature, whilst reverse tendency is detected with increasing Prandtl number and heat absorption parameter. Newtonian heating parameter and thermal and mass buoyancy forces boost fluid velocity, whilst Schmidt number and chemical reaction have the opposite impact. It is noteworthy to point out in this study that the velocity boundary layer thickness for the Newtonian fluid is larger than the Casson fluid.

1. Introduction

The study of non-Newtonian fluid flow models has fascinated investigators owing to its significant applications in chemical, pharmaceutical, and cosmic and food industries such as in the production of several chemicals, foams, oil, gas, paint, syrup, juice, chocolate, and many other food products. However, the study of non-Newtonian fluids is not as straightforward as Newtonian fluids, since there does not exist a single constructive equation for the non-Newtonian fluids that can be used to explicate them. In order to analyze their characteristics, a number of researchers introduced different constitutive equations or models. The foremost investigations [1–9] considered, respectively, are power law, second-grade, Jeffery, Maxwell, viscoplastic, Bingham plastic, Brinkman type, Oldroyd-B, and Walters-B fluid models. The trendiest Casson model was first introduced for the prediction of the flow narration of pigment oil suspensions of the printing ink type by Casson [10]. Subsequently, Mustafa et al. [11] studied unsteady boundary layer flow of a Casson fluid due to an impulsively started moving flat plate. Rao et al. [12] analyzed heat transfer in a Casson rheological fluid from a semi-infinite vertical plate with partial slip conditions. Khalid et al. [13] studied unsteady MHD free convection flow of Casson fluid past over an oscillating vertical plate embedded in a porous medium. Kataria and Patel [14] examined radiation and chemical reaction effects on MHD Casson fluid flow past an oscillating vertical plate embedded in a porous medium. Kataria and Patel [15] studied heat and mass transfer in MHD Casson fluid flow past over an oscillating vertical plate embedded in a porous medium with ramped wall temyperature. Mahanthesh et al. [16] studied the two-phase flow of dusty Casson fluid Cattaneo–Christov heat flux and heat source

past a cone, wedge, and plate. Shamshuddin et al. [17] analyzed chemical reaction effects on unsteady free convection radiated Casson fluid flow over an inclined porous plate numerically. Shamshuddin et al. [18] presented chemical reaction effects on thermosolutal micropolar fluid past a permeable stretching porous sheet. Shamshuddin et al. [19] examined radiation, heat source/sink effects on micropolar fluid flow due to a permeable stretching sheet with partial slip, and surface heat flux boundary conditions. Rajput et al. [20] studied numerically radiated Casson thermosolutal convective fluid flow over a vertical plate propagated by Arrhenius kinetics with heat source/sink.

In all these investigations, the conditions at the wall surface are commonly ramped, constant or variable wall temperature. However, there were several problems of physical interest where the heat is transported to the fluid via a bounding surface with a finite heat capacity. In this case, the above thermal boundary conditions fail to work; consequently, the Newtonian heating conditions are highly required. The applications of Newtonian heating are significant in heat exchangers, petroleum industry, turbines, and also in convective flows set up when the bounding surface absorbs heat by solar radiation. Merkin [21] first introduced the Newtonian heating condition in natural convection boundary layer flow over a vertical surface. Lesnic et al. [22, 23] studied free convection boundary layer flows along vertical and horizontal surfaces in a porous medium generated by Newtonian heating. Chaudhary and Jain [24] studied unsteady free convection boundary layer flow past an impulsively started vertical plate with Newtonian heating. Salleh et al. [25] studied forced convection boundary layer flow near the forward stagnation point of an infinite plane wall generated by Newtonian heating. Salleh et al. [26] discussed the impact of Newtonian heating on boundary layer flow and heat transfer over a stretching sheet. Hussanan et al. [27] performed an exact analysis of heat and mass transfer flow past a vertical plate in the presence of Newtonian heating. Hussanan et al. [28, 29] evaluated the influence of Newtonian heating on unsteady boundary layer flow by considering non-Newtonian and Newtonian fluids through the porous medium. Unsteady hydromagnetic natural convection flow past an impulsively moving vertical plate with Newtonian heating in a rotating framework was reported by Seth et al. [30]. Das et al. [31] analyzed the effects of Newtonian heating on MHD heat and mass transfer unsteady Casson fluid flow past a flat plate. Hussanan et al. [32] scrutinized the impact of Newtonian heating on heat transfer in the magneto-hydrodynamic flow of a Casson fluid through the porous medium. Recently, Prabhakar Reddy [33] evaluated the effect of Newtonian heating on a radiating hydromagnetic flow past an impulsively moving infinite vertical plate in the presence of Hall current.

In most of the studies mentioned above, the effects of viscous dissipation on the flow are ignored. On the other hand, in some cases, the fluid viscosity may experience a significant change with variation in the temperature and also, for the extreme size of flow field or at low temperature, the impact of viscous dissipation is essential. This type of flow takes place in many industrial applications such as the aerodynamic extrusion of plastic sheets, material handling conveyors, cooling or drying of papers and textiles, and glass fibre production. Due to these essential applications, the study of viscous dissipation on the flow becomes a special curiosity among many investigators. Mansour et al. [34] and Suneetha et al. [35] considered in their study the effect of viscous dissipation in MHD natural convection flow under different situations. Kumar [36] and Singh and Singh [37] scrutinized the impact of viscous dissipation in hydromagnetic flow through the stretching surface. Kishore et al. [38] analyzed the effects of thermal radiation and viscous dissipation on MHD heat and mass diffusion flow past an oscillating plate embedded in a porous medium with variable surface conditions. Pal et al. [39] studied convective-radiation effects on stagnation point flow of nanofluid over a stretching surface with viscous dissipation. Pal and Biswas [40] examined the viscous dissipation effects on mixed convective MHD oscillatory flow of Casson fluid in the presence of thermal radiation, chemical reaction, and Soret effect. Prabhakar Reddy [41] discussed viscous dissipation and mass transfer effects on unsteady MHD free convective flow of an incompressible past an infinite vertical porous plate. Zigta [42] analyzed the influence of viscous dissipation on hydromagnetic flow in between a pair of infinite vertical Couette channel walls in the presence of thermal radiation and chemical reaction. Shamshuddin et al. [43] studied dissipative radiated micropolar convective fluid from a rotating vertical plate with oscillatory plate velocity adjacent to a permeable medium numerically. Shamshuddin et al. [44] studied numerically rotating unsteady multiphysico-chemical magneto-micropolar flow in a porous medium from a vertical plate in the presence of Hall current. Shamshuddin and Tirupathi [45] carried out a numerical investigation for dissipative micropolar fluid flow past an inclined porous plate with heat source/sink. Ferdows et al. [46] studied micropolar fluid flow past a horizontal stretching sheet through a porous medium in the presence of Soret–Dufour effect and viscous dissipation. Prabhakar Reddy and Muthucumaraswamy [47] analyzed numerically the impact of viscous dissipation on MHD flow past an oscillating vertical porous plate with variable surface conditions in the presence of thermal radiation and chemical reaction.

The above comprehensive literature analysis motivated us to determine the impact of Newtonian heating effect on unsteady MHD Casson fluid past an oscillating vertical porous plate in the existence of thermal radiation, chemical reaction, heat sink, and viscous dissipation effects as this problem was not being discussed. This kind of exploration has several medical and industrial applications such as in the study of blood flow in the cardiovascular system, glass manufacturing, paper production, and purification of crude oil. The leading coupled nonlinear PDEs of the model have been solved numerically by adopting the finite difference method. This numerical approach coupled with the model problem, which in essence extends the previously published work of Das et al. [31] by including heat sink, surface porosity, and viscous dissipation effect, which comprise the novelty of the present study. Further, to validate the present

numerical procedure, a comparison was executed in the limiting conditions between the present results and earlier published works in the literature. It has been found significant conformity between the results, which provides the accuracy of the present results.

2. Mathematical Model

We consider an unsteady heat-absorbing Casson MHD free convection heat and mass transfer flow of viscous, incompressible electrically conducting fluid past a vertical porous plate oscillating in its own plane fixed at $y' = 0$, where y' is the coordinate axis normal to the plate as shown in Figure 1. The uniform magnetic field of strength B_0 applied in a transverse direction to the flow. The induced magnetic field formed by the motion of the fluid is neglected in comparison to the applied one as the magnetic Reynolds number is small enough. Initially, at time $t' = 0$, both the fluid and plate are at uniform temperature T_∞' and the concentration near to the plate C_∞'. At time $t' > 0$, the plate starts to oscillate in the vertical direction in its own plane with velocity $u' = U_0 \cos(\omega' t')$ against the gravitational field, where U_0 is the amplitude and ω' is the frequency of the plate oscillations. At the same time, between the local surface temperature T' and heat transfer from the plate, there is a direct proportionality relation and the concentration level near to the plate surface raised from C_∞' to C_w'. There are first-order chemical reactions existing between the diffusing species and the fluid. The viscous dissipation term is taken into account in the energy equation.

The rheological equation of the state for the isotropic and incompressible flow of a Casson fluid following Khalid et al. [13] and Hussanan et al. [28] is given as follows:

$$\tau = \tau_0 + \mu\alpha^*, \tag{1}$$

or

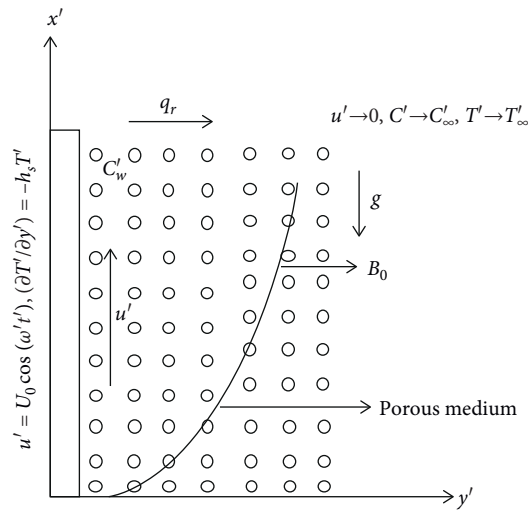

Figure 1: Schematic drawing of the model.

$$\tau_{ij} = \begin{cases} 2\left(\mu_B + \dfrac{p_y}{\sqrt{2\pi}}\right)e_{ij}, & \pi > \pi_c, \\ 2\left(\mu_B + \dfrac{p_y}{\sqrt{2\pi_c}}\right)e_{ij}, & \pi < \pi_c, \end{cases}, \tag{2}$$

where τ is the shear stress, τ_0 is the Casson yield stress, μ is the dynamic viscosity, α^* is the shear rate, $\pi = e_{ij}e_{ij}$ and e_{ij} is the $(i, j)^{\text{th}}$ component of the deformation rate, π is the product of the component of deformation rate with itself, π_c is the critical value of this product based on the non-Newtonian fluid model, μ_B is the plastic dynamic viscosity of the non-Newtonian fluid, and p_y is the yield stress of the fluid. By considering these mentioned assumptions, the governing system of PDEs of the model following Das et al. [31] and Hussanan et al. [32] is as follows:

$$\begin{aligned}
\frac{\partial u'}{\partial t'} &= \upsilon\left(1 + \frac{1}{\alpha}\right)\frac{\partial^2 u'}{\partial y'^2} - \frac{\sigma B_0^2 u'}{\rho} - \left(1 + \frac{1}{\alpha}\right)\frac{\upsilon\varphi}{k_1}u' + g\beta_T(T' - T_\infty') + g\beta_C(C' - C_\infty'), \\
\frac{\partial T'}{\partial t'} &= \frac{k}{\rho c_p}\frac{\partial^2 T'}{\partial y'^2} - \frac{1}{\rho c_p}\frac{\partial q_r}{\partial y'} - \frac{Q_0}{\rho c_p}(T' - T_\infty') + \frac{\upsilon}{c_p}\left(\frac{\partial u'}{\partial y'}\right)^2, \\
\frac{\partial C'}{\partial t'} &= D_m\frac{\partial^2 C'}{\partial y'^2} - k_r'(C' - C_w'),
\end{aligned} \tag{3}$$

where u' is the velocity of the fluid, g is the acceleration due gravity, β_T is the volumetric coefficient of thermal expansion, β_C is the volumetric coefficient of concentration expansion, T' is the temperature of the fluid, C' is the concentration of the fluid, k is the thermal conductivity, υ is the kinematic viscosity, μ is the fluid viscosity, ρ is the fluid density, σ is the electrical conductivity, c_p is the specific heat at constant pressure, q_r is the radiation heat flux, Q_0 is the heat absorption constant, k_r' is the chemical reaction constant, D_m chemical molecular diffusivity, φ is the porosity, k_1 is the permeability of the medium, and t' time.

The associated initial and boundary conditions of the illustrated model are as follows:

$$
\begin{aligned}
&t' < 0;\\
&u' = 0,\\
&T' = T'_\infty,\\
&C' = C'_\infty, \quad \text{for all } y' \geq 0,\\
&t' \geq 0;\\
&u' = U_0 \cos(\omega' t'),\\
&\frac{\partial T'}{\partial y'} = -h_s T',\\
&C' = C'_w, \quad \text{at } y' = 0,\\
&u' \longrightarrow 0,\\
&T' \longrightarrow T'_\infty,\\
&C' \longrightarrow C'_\infty, \quad \text{as } y' \longrightarrow \infty,
\end{aligned}
\tag{4}
$$

where h_s is the heat transfer coefficient.

The radiative heat flux q_r under the Rosseland approximation is given by the following equation:

$$
q_r = -\frac{4\sigma^*}{3k^*}\frac{\partial T'^4}{\partial y'}, \tag{5}
$$

where σ^* and k^* denote, respectively, the Stefan–Boltzmann constant and absorption coefficient. According to Das et al. [31], after simplifying T'^4, by employing the Taylor series, we obtain the following equation:

$$
T'^4 = 8T'^3_\infty T' - 3T'^4_\infty. \tag{6}
$$

Substituting equations (5) and (6) into equation (2), the energy equation reduces to

$$
\begin{aligned}
\frac{\partial T'}{\partial t\prime} = {} & \frac{k}{\rho c_p}\frac{\partial^2 T'}{\partial y'^2} + \frac{16\sigma^* T'^3_\infty}{3k^*\rho c_p}\frac{\partial^2 T'}{\partial y'^2}\\
& - \frac{Q_0}{\rho c_p}\left(T' - T'_\infty\right) + \frac{\upsilon}{c_p}\left(\frac{\partial u'}{\partial y'}\right)^2.
\end{aligned}
\tag{7}
$$

Introducing the following nondimensional variables and parameters, we obtain the following equation:

$$
\begin{aligned}
u &= \frac{u'}{U_0},\\
\tau &= \frac{t' U_0^2}{\upsilon},\\
\xi &= \frac{y' U_0}{\upsilon},\\
S_c &= \frac{\upsilon}{D_m},\\
P_r &= \frac{\upsilon \rho c_p}{k},\\
M &= \frac{\sigma B_0^2 \upsilon}{\rho U_0^2},\\
k_r &= \frac{\upsilon k'_r (C'_w - C'_\infty)}{U_0^2},\\
Q &= \frac{Q_0 \upsilon}{U_0^2 \rho c_p},\\
\omega &= \frac{\omega\prime \upsilon}{U_0^2},\\
N_r &= \frac{16\sigma^* T'^3_\infty}{3kk^*},\\
\frac{1}{K} &= \frac{\upsilon \varphi^2}{k_1 U_0^2},\\
\theta &= \frac{T' - T'_w}{T'_\infty},\\
\phi &= \frac{C\prime - C'_w}{C'_w - C'_\infty},\\
E_c &= \frac{U_0^2}{c_p T'_\infty},\\
G_r &= \frac{g\beta_T \upsilon T'_\infty}{U_0^3},\\
G_m &= \frac{g\beta_C \upsilon (C'_w - C'_\infty)}{U_0^3}.
\end{aligned}
\tag{8}
$$

Substituting equations (1) and (3) into (6), we obtain the dimensionless governing system of PDEs of the model as follows:

$$\frac{\partial u}{\partial \tau} = \left(1 + \frac{1}{\alpha}\right)\frac{\partial^2 u}{\partial \xi^2} - Mu - \left(1 + \frac{1}{\alpha}\right)\frac{u}{K} + G_r\theta + G_m C,$$
$$\frac{\partial \theta}{\partial \tau} = \frac{(1 + N_r)}{P_r}\frac{\partial^2 \theta}{\partial \xi^2} - Q\theta + E_c\left(\frac{\partial u}{\partial \xi}\right)^2, \tag{9}$$
$$\frac{\partial C}{\partial \tau} = \frac{1}{S_c}\frac{\partial^2 C}{\partial \xi^2} - k_r C.$$

The analogous initial and boundary conditions become

$$\begin{aligned}
&\tau < 0;\\
&u = 0,\\
&\theta = 0,\\
&C = 0, \quad \text{for all } \xi \geq 0,\\
&\tau \geq 0;\\
&u = \cos(\omega\tau),\\
&\frac{\partial \theta}{\partial \xi} = -\gamma(1 + \theta),\\
&C = 1 \text{at } \xi = 0,\\
&u \longrightarrow 0,\\
&\theta \longrightarrow 0,\\
&C \longrightarrow 0 \text{ as } \xi \longrightarrow \infty.
\end{aligned} \tag{10}$$

3. Numerical Procedure

The modeled systems of coupled nonlinear PDEs in equations (8)–(10) are solved with connected initial and boundary conditions of equation (11) In general, finding the exact solutions of these equations is not possible. Therefore, DuFort–Frankel's explicit finite difference technique is utilized to solve the governing system of equations (8)–(10) with related initial and boundary conditions of equation (11), which is quite easy, accurate, efficient, and unconditionally stable. The comprehensive elucidation of this numerical procedure was given in Jain et al. [48]. On applying the DuFort–Frankel's procedure to equations (8)–(10), it results in

$$\begin{aligned}
\left(\frac{u_{i,j+1} - u_{i,j-1}}{2\Delta\tau}\right) &= \left(1 + \frac{1}{\alpha}\right)\left(\frac{u_{i-1,j} - u_{i,j+1} - u_{i,j-1} + u_{i+1,j}}{(\Delta\xi)^2}\right) - \frac{M}{2}\left(u_{i,j+1} + u_{i,j-1}\right)\\
&\quad - \left(1 + \frac{1}{\alpha}\right)\frac{1}{2K}\left(u_{i,j+1} + u_{i,j-1}\right) + \frac{G_r}{2}\left(\theta_{i,j+1} + \theta_{i,j-1}\right) + \frac{G_m}{2}\left(C_{i,j+1} + C_{i,j-1}\right),\\
\left(\frac{\theta_{i,j+1} - \theta_{i,j-1}}{2\Delta\tau}\right) &= \frac{(1 + N_r)}{P_r}\left(\frac{\theta_{i-1,j} - \theta_{i,j+1} - \theta_{i,j-1} + \theta_{i+1,j}}{(\Delta\xi)^2}\right) - \frac{Q}{2}\left(\theta_{i,j+1} + \theta_{i,j-1}\right) + E_c\left(\frac{u_{i,j+1} - u_{i,j-1}}{2\Delta\xi}\right)^2,\\
\left(\frac{C_{i,j+1} - C_{i,j-1}}{2\Delta\tau}\right) &= \frac{1}{S_c}\left(\frac{C_{i-1,j} - C_{i,j+1} - C_{i,j-1} + C_{i+1,j}}{(\Delta\xi)^2}\right) - \frac{k_r}{2}\left(C_{i,j+1} + C_{i,j-1}\right).
\end{aligned} \tag{11}$$

The initial and boundary conditions of equation (11) can be expressed as follows:

$$\begin{aligned} u(i,0) &= 0, \\ \theta(i,0) &= 0, \\ C(i,0) &= 0, \quad \text{for all } i, \\ u(0,j) &= \cos(\omega\tau), \\ \frac{\theta(1,j)-\theta(0,j)}{2\Delta\xi} &= -\gamma(1+\theta(0,j)), \\ C(0,j) &= 1, \quad \text{for all } j, \\ u(\infty,j) &\longrightarrow 0, \\ \theta(\infty,j) &\longrightarrow 0, \\ C(\infty,j) &\longrightarrow 0 \quad \text{for all } j. \end{aligned} \tag{12}$$

Here, the suffix i corresponds to space ξ and the suffix j corresponds to time τ, $\Delta\xi$ is the mesh size along $\xi-$ direction, and $\Delta\tau$ is the mesh size along $\tau-$ direction. The physical domain of the problem is considered as finite restricted as the rectangle of finite dimensions for computational purpose. The finite difference equations (12) and (13) under the initial and boundary conditions (16) at every internal node on a particular j level constitute a tri-diagonal system of equations, which are solved by using Thomas algorithm. The free-stream boundary condition $\xi \longrightarrow \infty$ has been fixed by $\xi_{\max} = 4$, the value greater than 4 does not result in any significant change in the numerical values of $u(\xi,\tau)$, $\theta(\xi,\tau)$, and $C(\xi,\tau)$ under various key parameters. By fixing the mesh size $\Delta\tau = 0.01$, the developed code for the present numerical scheme was run with various mesh sizes $\Delta\xi = 0.001, 0.002$ and 0.009, where no substantial variation was detected in the numerical values of velocity u, temperature θ, and concentration C. Thus, the mesh size $\Delta\xi = 0.001$ has been fixed for the complete computational process.

Some essential physical quantities connected to the heat and mass transfer characteristics of the transport, such as the skin friction and Nusselt and Sherwood numbers, are defined in dimensionless form by the following equation:

$$\begin{aligned} C_f &= -\left(1+\frac{1}{\alpha}\right)\left(\frac{\partial u}{\partial \xi}\right)_{\xi=0}, \\ N_u &= -\left(\frac{\partial \theta}{\partial \xi}\right)_{\xi=0}, \\ S_h &= -\left(\frac{\partial C}{\partial \xi}\right)_{\xi=0}. \end{aligned} \tag{13}$$

3.1. Validation of the Present Numerical Procedure. In order to exhibit the validation and accuracy of the present numerical procedure, a comparison of the skin friction calculated in the present work and earlier published works of Das et al. [31] and Hussanan et al. [32] obtained analytically is provided in Table 1 when $\alpha \longrightarrow \infty$, $G_m = 0$, $M = 0, K \longrightarrow \infty, N_r = 0, Q = 0, E_c = 0$, and $C = 0$. It is perceived from Table 1 that there is an outstanding agreement among the results of Das et al. [31] and Hussanan et al. [32] obtained analytically and the present results obtained numerically by the developed code in this work. This entrusts the accuracy of the present numerical procedure.

4. Graphical Results and Discussion

To investigate the physical significance of the modeled problem, the influence of various key parameters involved in the problem such as magnetic parameter M, heat absorption parameter Q, radiation parameter N_r, Eckert number E_c, Newtonian heating parameter γ, Prandtl number P_r, Schmidt number S_c, chemical reaction rate k_r, porosity parameter K, phase angle $\omega\tau$, Casson parameter α, thermal Grashof number G_r, and mass Grashof number G_m on the fluid velocity, temperature, and concentration are evaluated numerically and executed graphically, whilst the skin friction and Nusselt and Sherwood numbers are put in tabular format. The numerical calculations have been done by adopting the default values of several involved parameters in the problem as $P_r = 0.71$, $N_r = 0.71$, $Q = 1$, $E_c = 0.01$, $\gamma = 0.4$, $S_c = 0.6$, $k_r = 0.5$, $G_r = 5$, $G_m = 4$, $M = 2$, $K = 0.5$, $\alpha = 1$, and $\omega\tau = \pi/3$ until otherwise specified particularly.

The variation of velocity and temperature distributions against ξ under the influence of Prandtl number P_r is shown in Figure 2 for mixture of noble gas ($P_r = 0.5$), air ($P_r = 0.71$), gas ($P_r = 1$), and water ($P_r = 7$). It is observed a decreasing effect on both velocity and temperature in the boundary layer as the Prandtl number increased. Physically, an increase in P_r leads to an increase of fluid viscosity, so that fluid becomes thick, and consequently, fluid velocity and temperature decrease. The effect of heat absorption parameter Q on fluid velocity and temperature against ξ is depicted in Figure 3. It is clearly seen that increasing values of heat absorption Q give lessening fluid temperature and velocity. Physically, when heat absorption is present in the energy equation, it absorbs energy and as a result declines the fluid temperature and consequently reduces fluid motion. Figure 4 exhibits the effect of radiation N_r on fluid velocity and temperature against ξ. It is seen that growing values of N_r improve the thickness of thermal and momentum boundary layers, which gives an increasing effect on both fluid motion and temperature. Figure 5 illustrates the variation of velocity and temperature distributions against ξ under the effect of Eckert number E_c. We found a rise in both velocity and temperature of the fluid with enhancement in E_c. Physically, increasing Eckert number E_c converts the kinetic energy into the internal energy, which causes to enhance both fluid velocity and temperature. The effect of Newtonian heating on fluid velocity and temperature against ξ is shown in Figure 6. A significant effect on both fluid velocity and temperature within the boundary layer is noticed. Increasing values of Newtonian heating

Table 1: Comparison of the skin friction coefficient calculated in the present work with published works.

G_r	P_r	γ	τ	$\omega\tau$	Das et al. [31] $(M = 0, G_m = 0)$	Hussanan et al. [32]	Present work $M = 0, K \longrightarrow \infty, Q = 0, E_c = 0, G_m = 0$
5	0.35	1	0.01	0	5.5818	5.5818	5.5818
10	—	—	—	—	5.5218	5.5218	5.5219
5	0.50	—	—	—	5.5956	5.5956	5.5956
-	0.35	2	—	—	5.5027	5.5027	5.5027
-	—	1	0.02	—	3.8620	3.8620	3.8620
-	—	—	0.01	$\pi/2$	4.4819	4.4819	4.4819

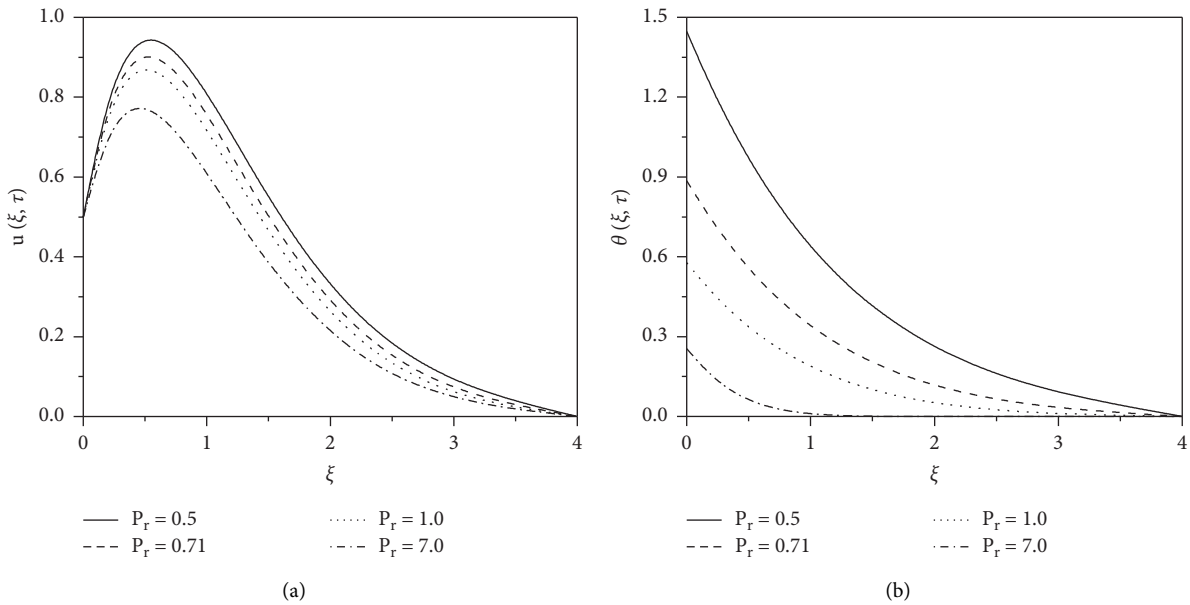

Figure 2: Variation of (a) velocity $u(\xi, \tau)$ and (b) temperature $\theta(\xi, \tau)$ against ξ for various values of P_r.

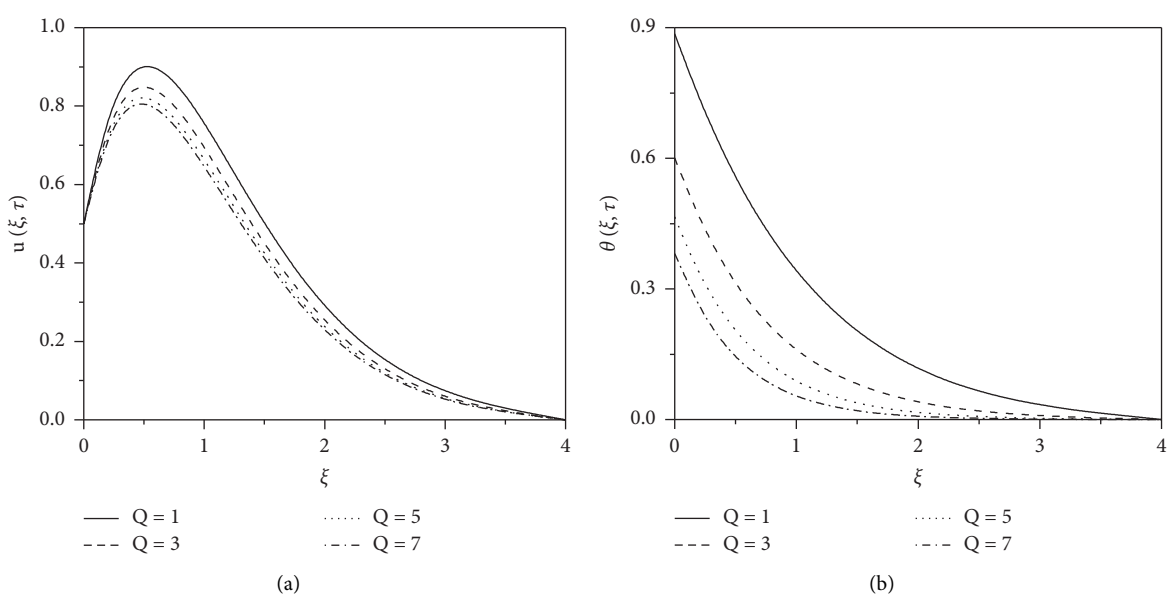

Figure 3: Variation of (a) velocity $u(\xi, \tau)$ and (b) temperature $\theta(\xi, \tau)$ against ξ for various values of Q.

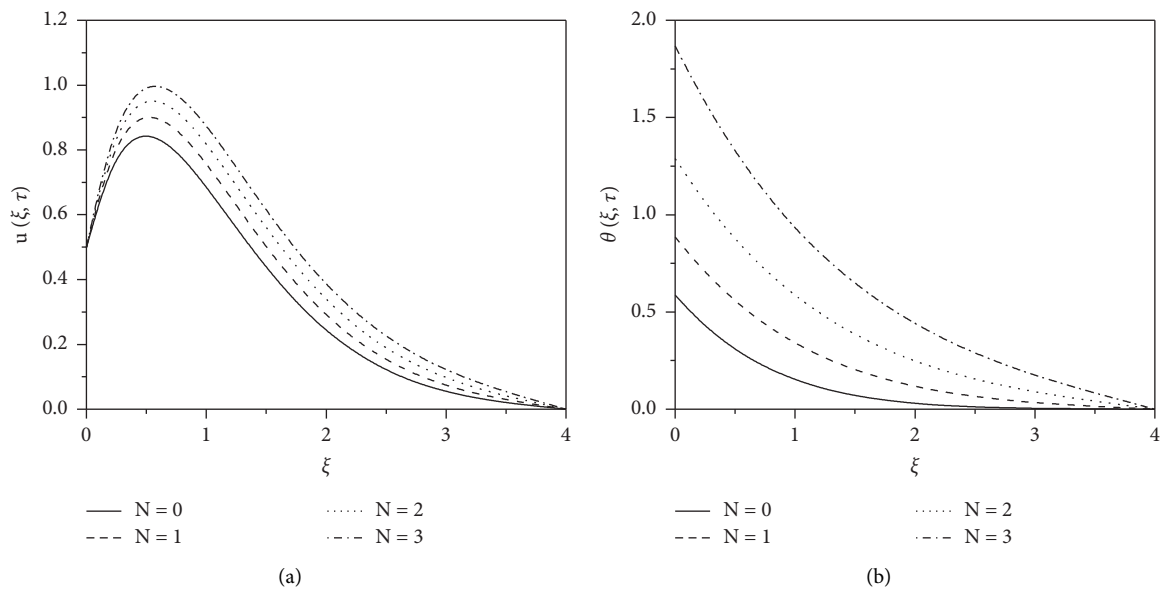

Figure 4: Variation of (a) velocity $u(\xi, \tau)$ and (b) temperature $\theta(\xi, \tau)$ against ξ for various values of N_r.

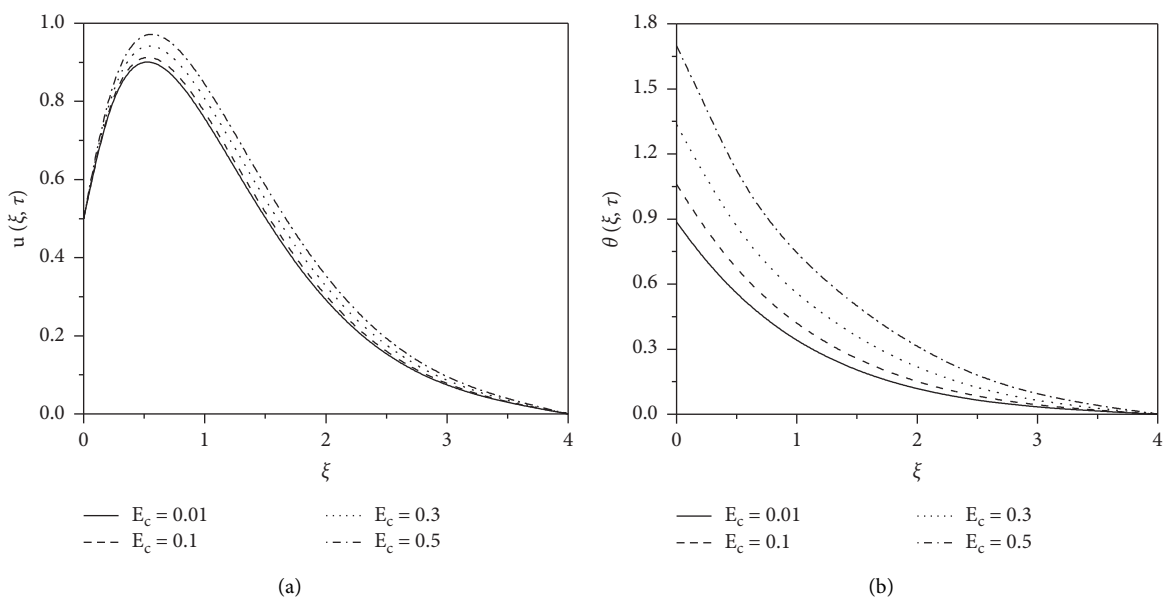

Figure 5: Variation of (a) velocity $u(\xi, \tau)$ and (b) temperature $\theta(\xi, \tau)$ against ξ for various values of E_c.

parameter γ reduce the fluid density and amplify the surface temperature of the plate, and as a result, fluid velocity and temperature increase. Figure 7 depicts the effect of Schmidt number S_c on the velocity and concentration distributions against ξ. By the definition, Schmidt number S_c is the relative influence of momentum diffusion on species diffusion. The momentum diffusion is quicker than species when $S_c > 1$, and opposite is true when $S_c < 1$. When $S_c = 1$, both momentum and species boundary layers are of the same order of magnitude. As expected, when values of S_c are increased, both fluid concentration and velocity fall down due to increasing momentum being diffused at a slighter rate than species. Figure 8 is plotted to show the variation of velocity and concentration distributions against ξ for various values of chemical reaction rate k_r. It is observed that a decreasing effect on both fluid velocity and concentration with enhancing values of chemical reaction rate. This is because increasing values of k_r reduce the chemical molecular diffusivity, and as a result, fluid concentration lessens therefore fluid velocity decreases. Figure 9 displays the effect of thermal Grashof number G_r and mass Grashof number G_m on the velocity distribution against ξ. It is clearly seen a remarkable increasing effect on the fluid velocity near to the plate surface and then starts to decline and receive the stationary position in the free stream with an increase in either G_r or G_m. By the definition, G_r is the ratio of thermal buoyancy force to the viscous

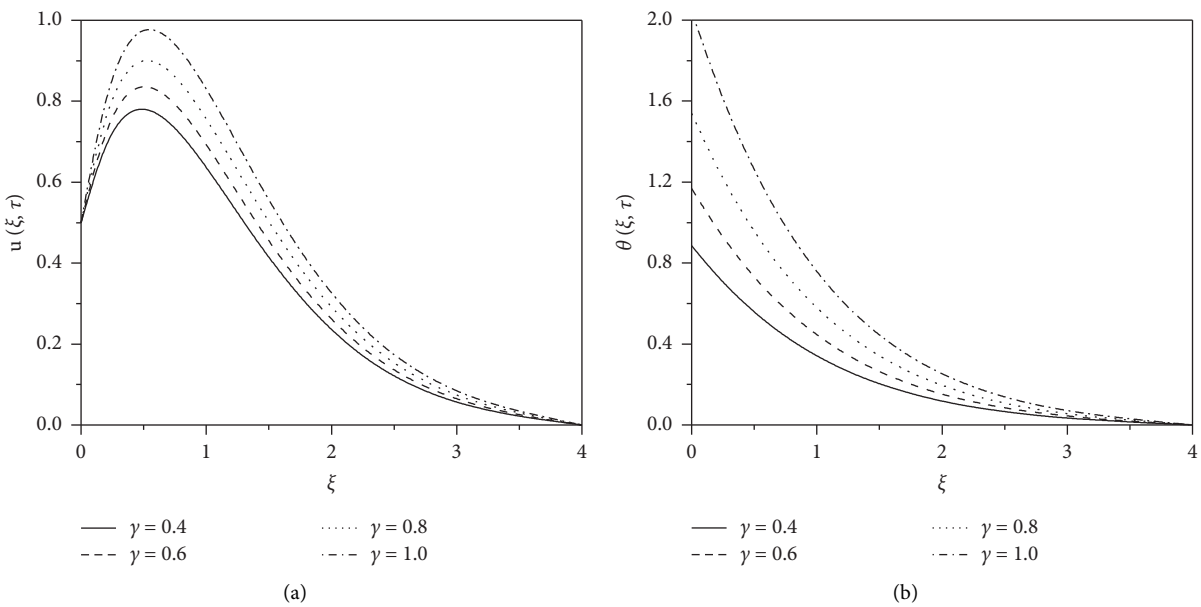

Figure 6: Variation of (a) velocity $u(\xi, \tau)$ and (b) temperature $\theta(\xi, \tau)$ against ξ for various values of γ.

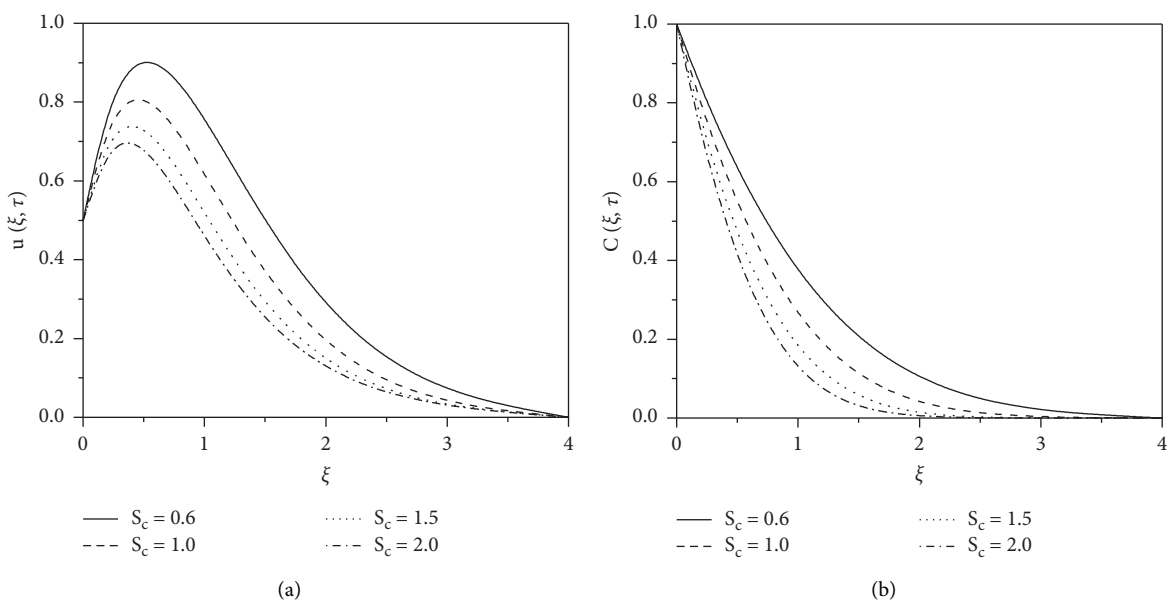

Figure 7: Variation of (a) velocity $u(\xi, \tau)$ and (b) concentration $C(\xi, \tau)$ against ξ for various values of S_c.

hydrodynamic force and G_m is the ratio of species buoyancy force to the viscous hydrodynamic force acting on the fluid transport. Increasing in either G_r or G_m causes to decrease in viscous hydrodynamic forces and consequently, the momentum of the fluid is higher. The effects of magnetic parameter M and permeability parameter K on the fluid velocity against ξ are illustrated in Figure 10. It is seen from Figure 10(a) that a decreasing effect on the fluid velocity with raising values of M and the reverse effect is noted on the fluid velocity with increasing values of K in Figure 10(b). When the applied magnetic field is active against the fluid motion, the strength of the Lorentz force is maximum and consequently, fluid motion decreases. An increase in the values of K furnishes reduction in the resistance of the porous medium as a result accelerates the fluid motion. Figure 11 elucidates the effects of Casson parameter α and phase angle $\omega\tau$ on the velocity against ξ. It is observed from Figure 11(a) that an increase in Casson fluid parameter α tend to decrease in the fluid motion. Physically, an increase in α causes to increase of plasticity of the fluid and consequently, fluid motion decreases. Figure 11(b) exposed that the fluid behavior is

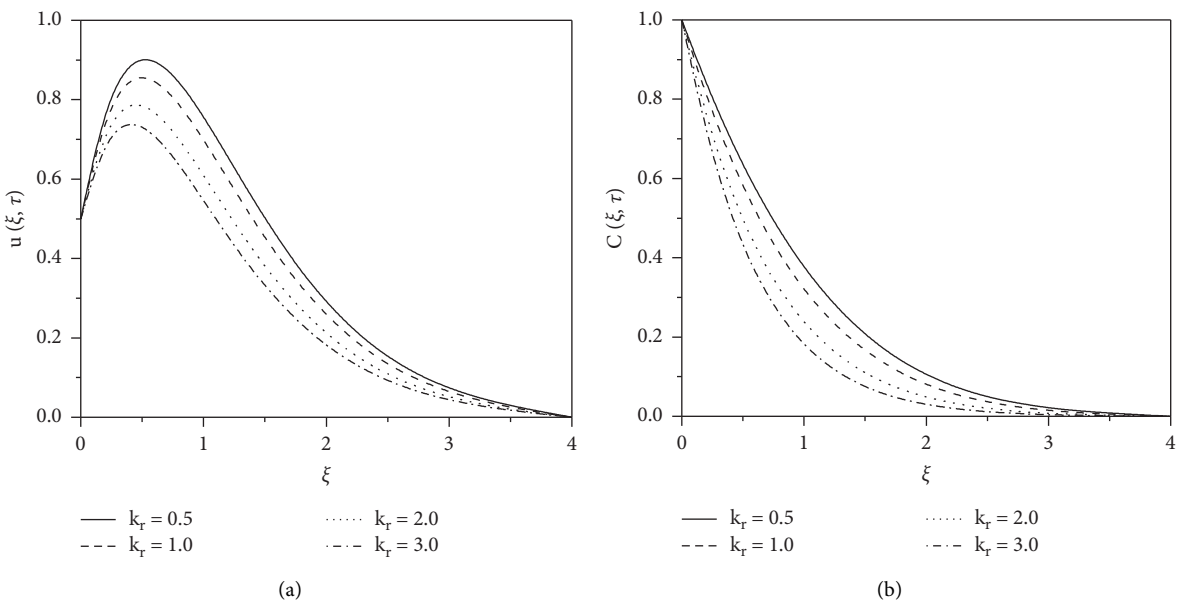

Figure 8: Variation of (a) velocity $u(\xi, \tau)$ and (b) concentration $C(\xi, \tau)$ against ξ for various values of k_r.

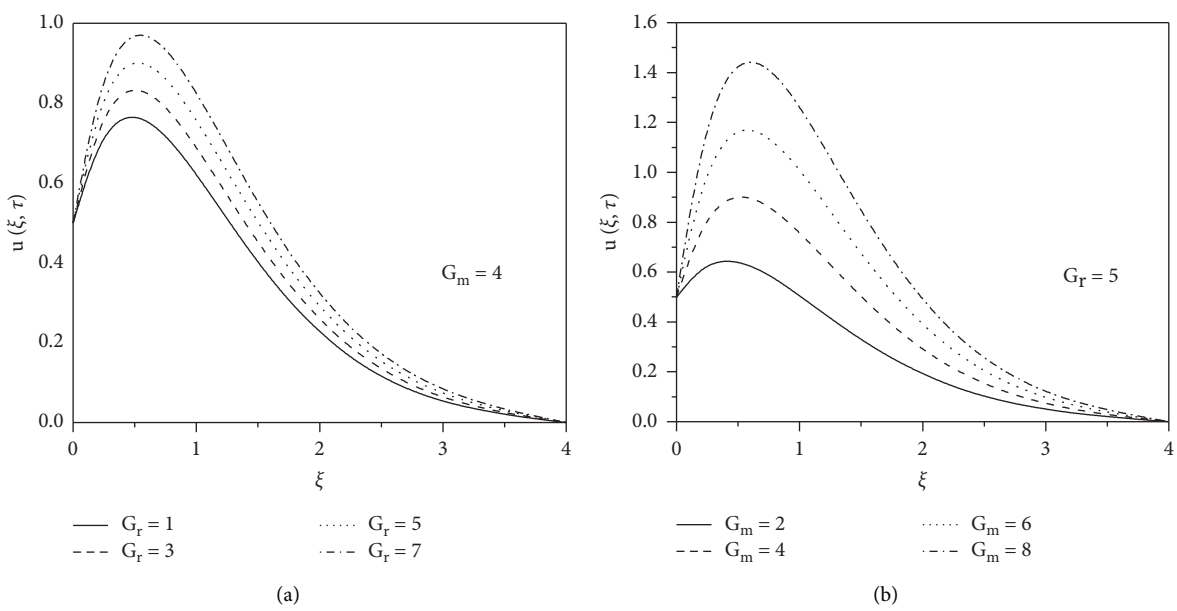

Figure 9: Variation of velocity $u(\xi, \tau)$ against ξ for various values of (a) G_r and (b) G_m.

an oscillatory near to the plate surface and these oscillations diminish away from the plate surface and finally, approach to zero as $\xi \longrightarrow \infty$.

Figures 12–14 accentuate the velocity distribution under the influence of $N_r, Q, S_c.k_r, M$, and γ against ξ in the limiting case when $\alpha \longrightarrow \infty$. Figures 12(a) and 14(b) revealed that the increasing effect is noted in the fluid motion with an increase in N_r and γ, whereas overturn is noted in the fluid motion from Figures 12(b), 13(a), 13(b), and 14(a). It is further observed that when Casson parameter $\alpha \longrightarrow \infty$, the non-Newtonian property of the fluid fully vanishes and the fluid behaves just like a Newtonian fluid. We conclude from these results that the velocity boundary layer thickness for the Newtonian fluid is larger than the Casson fluid.

The computed numerical results of the skin friction and Nusselt and Sherwood numbers are listed in Tables 2–4 respectively. It is clearly seen from Table 2 that there is a rise in the skin friction with an enhancement in values of radiation parameter, Eckert number, Newtonian heating parameter, porosity parameters, and thermal and mass Grashof numbers, whilst reverse tendency is perceived when the values of Prandtl number, heat absorption parameter, Schmidt number, chemical reaction rate, magnetic parameter, phase angle,

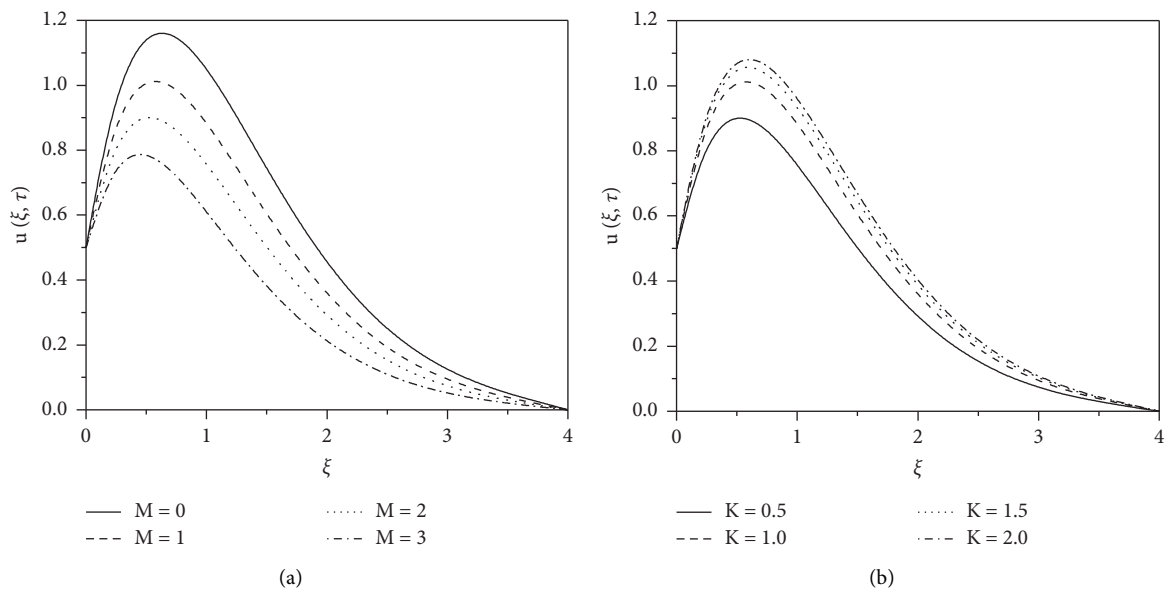

Figure 10: Variation of velocity $u(\xi, \tau)$ against ξ for various values of (a) M and (b) K.

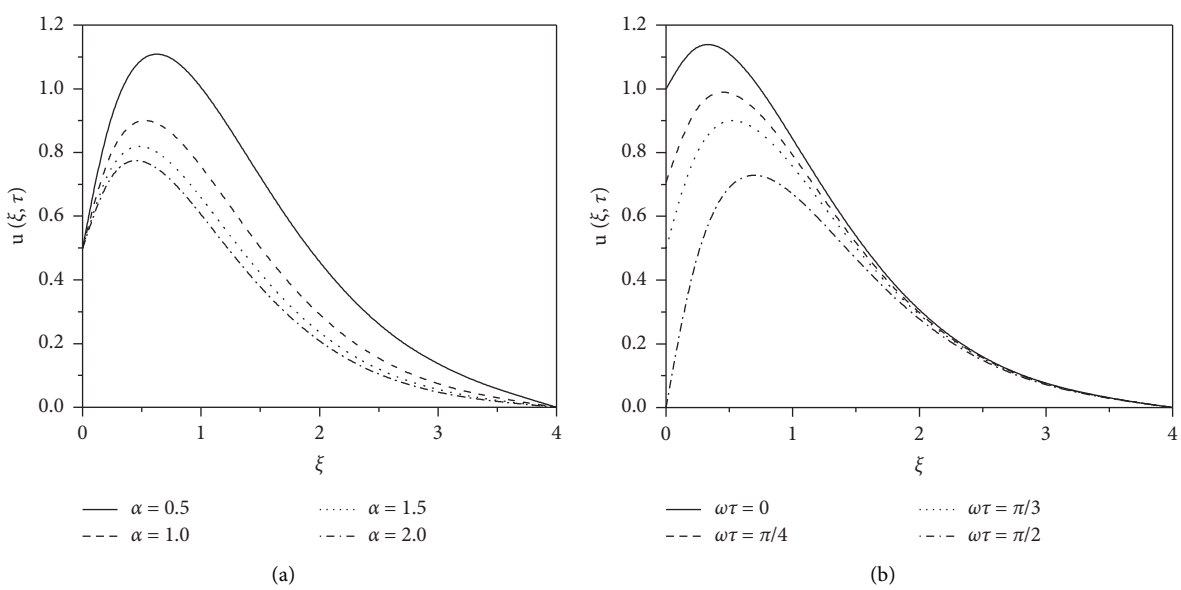

Figure 11: Variation of velocity $u(\xi, \tau)$ against ξ for various values of (a) α and (b) $\omega\tau$.

and Casson parameter are increased. Table 3 lists that the Nusselt number increases with growing values of radiation parameter, Eckert number, Newtonian heating parameter, and time, whilst opposite behavior is noticed when the Prandtl number and heat absorption parameter are increased. It is professed from Table 4 that an increase in Schmidt number and chemical reaction rate tends to ascend Sherwood number, whilst overturn is noticed with time progression. Further, there is an excellent agreement between the numerical values of Sherwood number computed numerically in

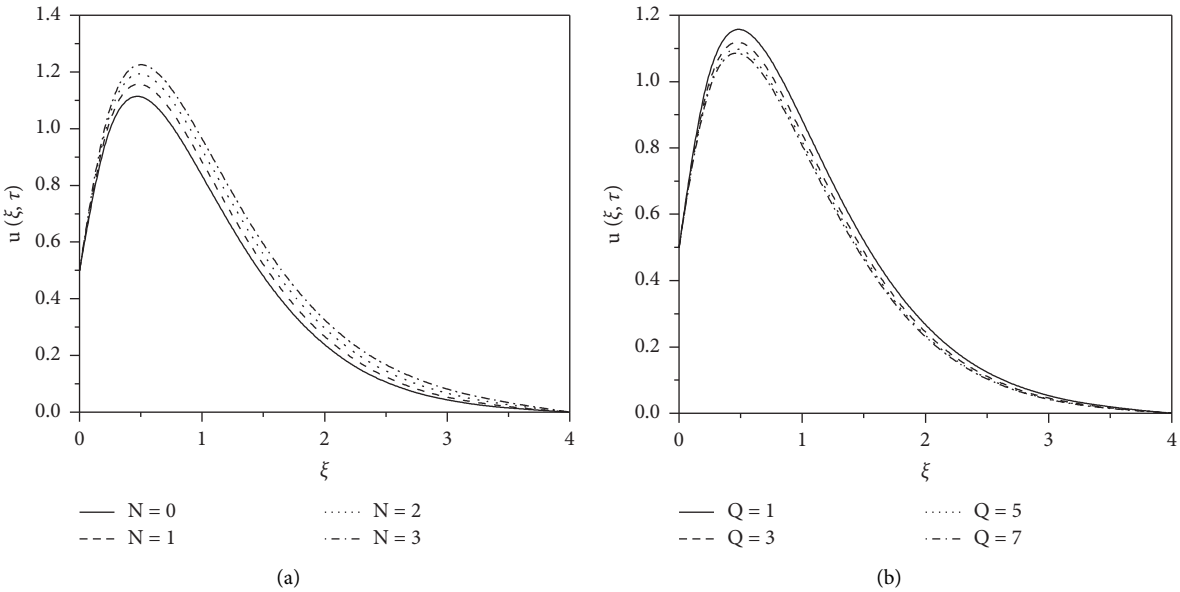

Figure 12: Variation of velocity $u(\xi, \tau)$ against ξ in the limiting case for various values of (a) N_r and (b) Q.

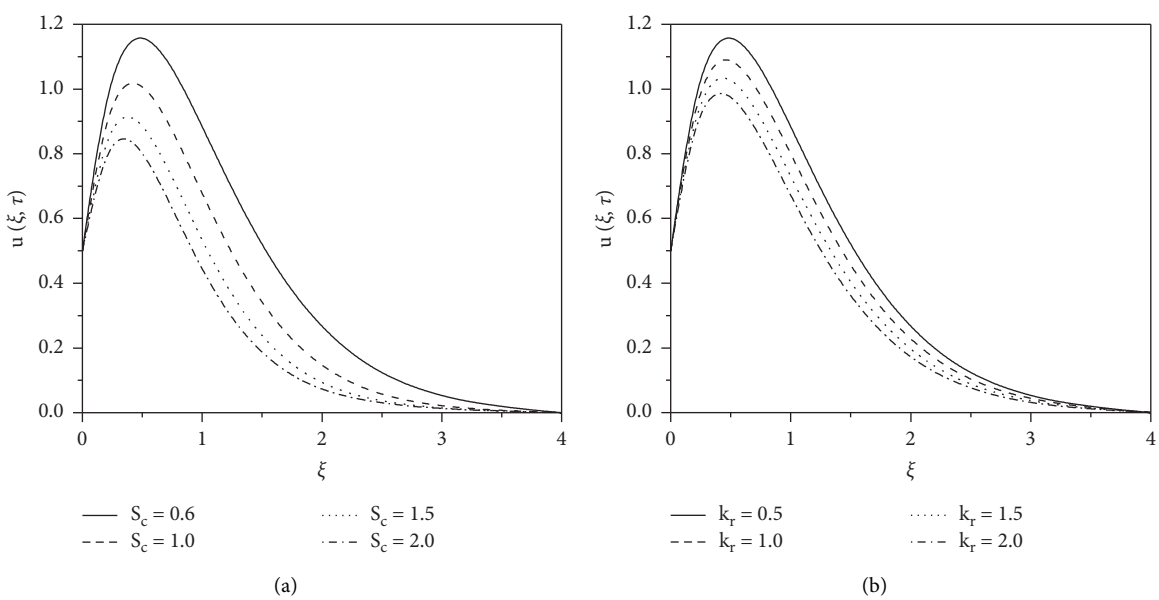

Figure 13: Variation of velocity $u(\xi, \tau)$ against ξ in the limiting case for various values of (a) S_c and (b) k_r.

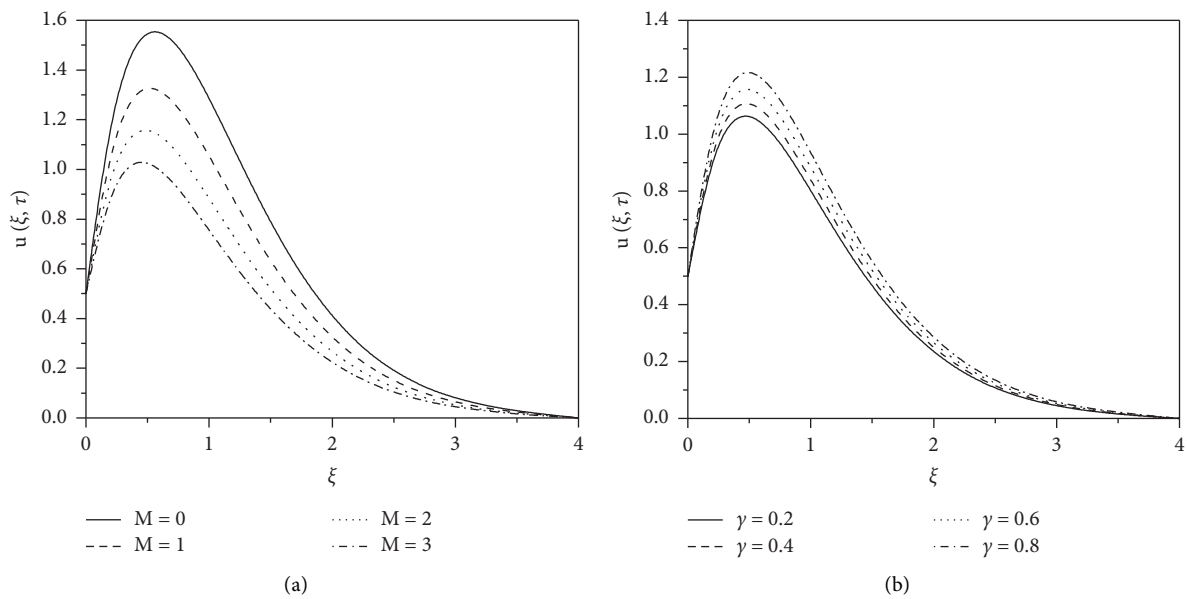

Figure 14: Variation of velocity $u(\xi, \tau)$ against ξ in the limiting case for various values of (a) M and (b) γ.

Table 2: Variation of skin friction C_f under the various physical parameters.

P_r	N_r	Q	E_c	γ	S_c	k_r	G_r	G_m	M	K	$\omega\tau$	α	C_f
0.71	1	1	0.01	0.4	0.6	0.5	5	4	2	0.5	$\pi/3$	1	1.574129
0.5	—	—	—	—	—	—	—	—	—	—	—	—	1.917861
0.71	**2**	—	—	—	—	—	—	—	—	—	—	—	2.025672
—	1	**3**	—	—	—	—	—	—	—	—	—	—	0.817608
—	—	1	**0.3**	—	—	—	—	—	—	—	—	—	2.217505
—	—	—	0.01	**0.6**	—	—	—	—	—	—	—	—	1.983211
—	—	—	—	0.4	**1**	—	—	—	—	—	—	—	0.486648
—	—	—	—	—	0.6	**1**	—	—	—	—	—	—	0.521087
—	—	—	—	—	—	0.5	**7**	—	—	—	—	—	2.659301
—	—	—	—	—	—	—	5	**6**	—	—	—	—	2.906206
—	—	—	—	—	—	—	—	4	**3**	—	—	—	0.095966
—	—	—	—	—	—	—	—	—	2	**1**	—	—	1.905461
—	—	—	—	—	—	—	—	—	—	0.5	$\pi/4$	—	0.864782
—	—	—	—	—	—	—	—	—	—	—	$\pi/3$	**1.5**	0.488020

Bold values represent the variation of the physical parameter.

Table 3: Variation of the Nusselt number N_u under various physical parameters.

P_r	N_r	Q	E_c	γ	τ	N_u
0.71	1	1	0.01	0.4	0.3	2.234581
0.5	—	—	—	—	—	3.229420
0.71	**2**	—	—	—	—	2.746519
—	1	**3**	—	—	—	2.090764
—	—	1	**0.3**	—	—	3.005701
—	—	—	0.01	**0.6**	—	3.976809
—	—	—	—	0.4	**0.5**	2.784050

Bold values represent the variation of the physical parameter.

Table 4: Comparison of the Sherwood number S_h calculated in the present work with the published work of Das et al. [31].

τ	S_c	k_r	Das et al. [31]	Present work
0.3	2	0.5	1.669937	1.669937
0.5	—	—	1.399282	1.399282
0.7	—	—	1.269245	1.269245
—	**1**	—	0.776503	0.776504
—	**2**	—	1.023319	1.023319
—	**3**	—	1.233626	1.233626
—	2	**0.1**	0.457642	0.457642
—	—	**0.5**	1.023319	1.023320
—	—	**1**	1.447192	1.447192

the present work and previously published work of Das et al. [31] computed analytically, which provides the exactness of our present results.

5. Conclusions

In this article, the governing system of PDEs of the model is analyzed numerically to determine the impact of Newtonian heating on unsteady heat-absorbing free convection MHD Casson dissipative fluid flow of radiating and reacting past an oscillating vertical porous plate. Lastly, this study can be further extended to include the Soret–Dufour effect in the presence of different boundary conditions, which is momentous when the density variation exists in the transport. Also, such analysis is essential in the context of geosciences, oceanography, and chemical engineering. The major concluding observations of this analysis can be summarized as follows:

1. The velocity and temperature increase with rising values of N_r, E_c, and γ, while an increase in P_r and Q have opposite effect.
2. An increase in S_c causes to decline velocity and concentration, while reverse effect is noticed when k_r is increased.
3. Increasing K, G_r, and G_m escalates the velocity, while increasing M, α, and $\omega\tau$ have opposite effect.
4. Skin friction decreases with growing values of $P_r, Q, S_c, k_r, M, \alpha$, and $\omega\tau$, while it raises with increasing values of N_r, E_c, γ, K, G_r, and G_m.
5. Nusselt number increases with increasing N_r, E_c, γ, and τ, while it reduces with increasing P_r and Q.
6. Increasing S_c and k_r enhances Sherwood number, while it lessens with progression of τ.

Data Availability

The data used to support the findings of this research are available within the article. This kind of investigation has several medical and industrial applications such as in the study of blood flow in the cardiovascular system, glass manufacturing, paper production, and purification of crude oil.

Conflicts of Interest

The authors declare that they have no conflicts of interest.

Acknowledgments

The authors are grateful to the management of the University of Dodoma, Tanzania, for the encouragement.

References

[1] B. I. Olajuwon, "Flow and natural convection heat transfer in a power law fluid a past a vertical plate with heat generation," *Journal of Nonlinear Science*, vol. 7, pp. 50–56, 2009.

[2] T. Hayat, I. Khan, R. Ellahi, and C. Fetecau, "Some MHD flows of a second grade fluid through the porous medium," *Journal of Porous Media*, vol. 11, no. 4, pp. 389–400, 2008.

[3] M. Qasim, "Heat and mass transfer in a Jeffrey fluid over a stretching sheet with heat source/sink," *Alexandria Engineering Journal*, vol. 52, no. 4, pp. 571–575, 2013.

[4] I. Khan, A. Farhad, U. H. Sami, and S. Sharidan, "Exact solutions for unsteady MHD oscillatory flow of Maxwell fluid in a porous medium," *Zeitschtift Fur Naturforschung*, vol. 68, pp. 635–645, 2013.

[5] M. A. Hassan, M. Pathak, and M. K. Khan, "Natural convection of viscopastic fluids in a square enclosure," *Journal of Heat Transfer*, vol. 135, no. 12, Article ID 122501, 2013.

[6] J. Kleppe and W. J. Marner, "Transient free convection in a Bingham plastic on a vertical flat plate," *Journal of Heat Transfer*, vol. 94, no. 4, pp. 371–376, 1972.

[7] M. N. Zakaria, H. Abid, I. Khan, and S. Sharidan, "The effects of radian on free convection flow with ramped wall temperature in Brinkman type fluid," *Journal of Teknologi*, vol. 62, pp. 33–39, 2013.

[8] I. Khan, K. Fakhar, and M. Anwar, "Hydromagnetic rotating flows of an oldroyd-b fluid in a porous medium," *Special Topics & Reviews in Porous Media - An International Journal*, vol. 3, no. 1, pp. 89–95, 2012.

[9] I. Khan, A. Farhad, S. Sharidan, and M. Qasim, "Unsteady free convection flow in a Walters-B fluid and heat transfer analysis," *Bull. Malaysian Math. Sci. Society*, vol. 37, no. 2, pp. 437–448, 2014.

[10] N. Casson, *A Flow Equation for Pigment Oil Suspensions of the Printing Ink in Rheology of Disperse Systems*, C. C. Mill, Ed., pp. 84–102, Pergamon Press, Oxford, UK, 1959.

[11] M. Mustafa, T. Hayat, I. Pop, and A. Aziz, "Unsteady boundary layer flow of a Casson fluid due to an impulsively started moving flat plate," *Heat Transfer - Asian Research*, vol. 40, pp. 553–576, 2011.

[12] A. S. Rao, V. R. Prasad, N. B. Reddy, and O. A. Beg, "Heat transfer in a Casson rheological fluid from a semi-infinite vertical plate with partial slip," *Heat Transfer - Asian Research*, vol. 44, pp. 1–20, 2013.

[13] A. Khalid, I. Khan, A. Khan, and S. Shafie, "Unsteady MHD free convection flow of Casson fluid past over an oscillating vertical plate embedded in a porous medium," *Engineering Science and Technology, an International Journal*, vol. 18, no. 3, pp. 309–317, 2015.

[14] H. R. Kataria and H. R. Patel, "Radiation and chemical reaction effects on MHD Casson fluid flow past an oscillating vertical plate embedded in porous medium," *Alexandria Engineering Journal*, vol. 55, no. 1, pp. 583–595, 2016.

[15] H. Kataria and H. Patel, "Heat and mass transfer in magnetohydrodynamic (MHD) Casson fluid flow past over an oscillating vertical plate embedded in porous medium with ramped wall temperature," *Propulsion and Power Research*, vol. 7, no. 3, pp. 257–267, 2018.

[16] B. Mahanthesh, O. D. Makinde, B. J. Gireesha, K. L. Krupalakshmi, and I. L. Animasaun, "Two-phase flow of dusty Casson fluid with cattaneo-christov heat flux and heat source past a cone, wedge and plate," *Defect and Diffusion Forum*, vol. 387, pp. 625–639, 2018.

[17] M. D. Shamshuddin, S. R. Mishra, and T. Tirupathi, "Chemically reacting radiative Casson fluid flow over an inclined porous plate: a numerical study," *Lecture Notes in Mechanical Engineering*, Springer, Singapore, 2019.

[18] M. D. Shamshuddin, T. Thumma, and S. R. Mishra, "Thermosolutal chemically reacting micropolar fluid past a permeable stretching porous sheet," *Defect and Diffusion Forum*, vol. 392, pp. 42–59, 2019.

[19] M. D. Shamshuddin, T. Tirupathi, and P. V. Satyanarayana, "Influence of heat source/sink on micro-polar fluid flow induced due to a permeable stretching sheet with partial slip and surface heat flux boundary conditions," *Journal of Applied and Computational Mechanics*, vol. 5, no. 5, pp. 816–826, 2019.

[20] G. R. Rajput, M. Shamshuddin, and S. O. Salawu, "Thermosolutal convective non-Newtonian radiative Casson fluid transport over a vertical plate propagated by Arrhenius kinetics with heat source/sink," *Heat Transfer*, vol. 50, no. 3, pp. 2829–2848, 2020.

[21] J. H. Merkin, "Natural-convection boundary-layer flow on a vertical surface with Newtonian heating," *International Journal of Heat and Fluid Flow*, vol. 15, no. 5, pp. 392–398, 1994.

[22] D. Lesnic, D. B. Ingham, and I. Pop, "Free convection boundary-layer flow along a vertical surface in a porous medium with Newtonian heating," *International Journal of Heat and Mass Transfer*, vol. 42, no. 14, pp. 2621–2627, 1999.

[23] D. Lesnic, D. B. Ingham, and I. Pop, "Free convection flow from a horizontal surface in a porous medium with Newtonian heating," *Porous Media*, vol. 3, pp. 227–235, 2000.

[24] R. C. Chaudhary and P. Jain, "Unsteady free convection boundary layer flow past an impulsively started vertical plate with Newtonian heating," *Romanian Journal of Physics*, vol. 51, pp. 911–925, 2006.

[25] M. Z. Salleh, R. Nazar, and I. Pop, "Forced convection boundary layer flow at a forward stagnation point with Newtonian heating," *Chemical Engineering Communications*, vol. 196, no. 9, pp. 987–996, 2009.

[26] M. Z. Salleh, R. Nazar, and I. Pop, "Boundary layer flow and heat transfer over a stretching sheet with Newtonian heating," *Journal of the Taiwan Institute of Chemical Engineers*, vol. 41, no. 6, pp. 651–655, 2010.

[27] A. Hussanan, I. Khan, and S. Shafie, "An exact analysis of heat and mass transfer past a vertical plate with Newtonian heating," *Journal of Applied Mathematics*, vol. 2013, Article ID 434571, 9 pages, 2013.

[28] A. Hussanan, M. Zuki Salleh, R. M. Tahar, and I. Khan, "Unsteady boundary layer flow and heat transfer of a Casson fluid past an oscillating vertical plate with Newtonian heating," *Plos one*, vol. 9, no. 10, Article ID e108763, 2014.

[29] A. Hassanan, Z. Ismail, I. Khan, A. G. Hussein, and S. Shafie, "Unsteady boundary layer MHD free convection flow in a porous medium with constant mass diffusion and Newtonian heating," *The European Physical Journal Plus*, vol. 129, p. 46, 2014.

[30] G. Seth, S. Sarkar, and R. Nandkeolyar, "Unsteady hydromagnetic natural convection flow past an impulsively moving vertical plate with Newtonian heating in a rotating system," *Journal of Applied Fluid Mechanics*, vol. 8, no. 3, pp. 623–633, 2015.

[31] M. Das, R. Mahato, and R. Nandkeolyar, "Newtonian heating effect on unsteady hydromagnetic Casson fluid flow past a flat plate with heat and mass transfer," *Alexandria Engineering Journal*, vol. 54, no. 4, pp. 871–879, 2015.

[32] A. Hussanan, M. Z. Salleh, I. Khain, and R. M. Tahar, "Heat transfer in magneto-hydrodynamic flow of a Casson fluid with porous medium and Newtonian heating," *Journal of Nanofluids*, vol. 6, pp. 1–10, 2017.

[33] B. Prabhakar Reddy, "Effect of Hall current on radiating hydromagnetic flow past an impulsively moving vertical porous plate with Newtonian heating," *I-Manager's Journal on Future Engineering and Technology*, vol. 15, no. 3, pp. 1–10, 2020.

[34] M. A. Mansour, N. F. Ei Ansary, and A. M. Aly, "Effect of chemical reaction and viscous dissipation on MHD natural convection flow saturated in a porous media with suction/injection," *International Journal of Applied Mathematics and Mechanics*, vol. 4, no. 2, pp. 60–76, 2008.

[35] S. Suneetha, N. Reddy, and V. Prasad, "Radiation and mass transfer effects on MHD free convection flow past an impulsively started isothermal vertical plate with dissipation," *Thermal Science*, vol. 13, no. 2, pp. 171–181, 2009.

[36] H. Kumar, "Radiative heat transfer with hydro-magnetic flow and viscous dissipation over a stretching surface in the presence of variable heat flux," *Thermal Science*, vol. 13, no. 2, pp. 163–169, 2009.

[37] P. K. Singh and J. Sing, "MHD flow with viscous dissipation and chemical reaction over a stretching porous plate in a porous medium," *International Journal of Engineering Research in Africa*, vol. 2, no. 2, pp. 1556–1564, 2012.

[38] P. M. Kishore, V. Rajesh, and V. Verma, "The effects of thermal radiation and viscous dissipation on MHD heat and mass diffusion flow past an oscillating vertical plate embedded in a porous medium with variable surface conditions," *Theoretical and Applied Mechanics*, vol. 39, no. 2, pp. 99–125, 2012.

[39] D. Pal, K. Vajravelu, and G. Mandal, "Convective-radiation effects on stagnation point flow of nanofluid over a stretching surface with viscous dissipation," *Journal of Mechanisms*, vol. 3, no. 30, pp. 289–297, 2014.

[40] D. Pal and S. Biswas, "Influence of chemical reaction and Soret effect on mixed convective MHD oscillatory flow of Casson fluid with thermal radiation and viscous dissipation," *International Journal of Algorithms, Computing and Mathematics*, vol. 3, no. 3, pp. 1897–1919, 2016.

[41] B. Prabhakar Reddy, "Mass transfer effects on an unsteady MHD free convective flow of an incompressible viscous dissipative fluid past an infinite vertical porous plate," *International Journal of Applied Mechanics and Engineering*, vol. 21, no. 1, pp. 143–155, 2016.

[42] B. Zigta, "Effects of thermal radiation, chemical reaction and viscous dissipation on MHD flow," *International Journal of Applied Mechanics and Engineering*, vol. 23, no. 4, pp. 787–801, 2018.

[43] M. D. Shamshuddin, O. A. Beg, and A. Kadir, "Finite element analysis of rotating oscillatory magneto-convective radiative micro-polar thermo-solutal flow," *International Journal of Fluid Mechanics Research*, vol. 45, no. 2, pp. 479–508, 2018.

[44] M. D. Shamshuddin, O. A. Beg, S. S. Reddy, and A. Kadir, "Rotating unsteady multi-physico-chemical magneto-micro-polar transport in porous media: galerkin finite element study," *Computational Thermal Sciences: International Journal*, vol. 10, no. 2, pp. 167–197, 2018.

[45] M. D. Shamshuddin and T. Tirupathi, "Numerical study of a dissipative micropolar fluid flow past an inclined porous plate with heat source/sink," *Propulsion and Power Research*, vol. 8, no. 1, pp. 56–68, 2018.

[46] M. Ferdows, M. Shamshuddin, and K. Zaimi, "Dissipative-radiative micropolar fluid transport in a non-Darcy porous medium with cross-diffusion effects," *CFD Letters*, vol. 12, no. 7, pp. 70–89, 2020.

[47] B. Prabhakar Reddy and R. Muthucumaraswamy, "Effects of thermal radiation on MHD chemically reactive flow past an oscillating vertical porous plate with variable surface conditions and viscous dissipation, i-manager's," *Journal on Future Engineering and Technology*, vol. 15, no. 2, pp. 8–18, 2020.

[48] M. K. Jain, S. R. K. Iyengar, and R. K. Jain, *Computational Methods for Partial Differential Equations*, Wiley Eastern Limited, Hoboken, NJ, USA, 1994.